A study of sound transmission in an abstract middle ear using physical and finite element models

Antonio Gonzalez-Herrera
Department of Civil Engineering, Materials and Fabrication, University of Malaga, Spain

Elizabeth S. Olson[a)]
Department of Otolaryngology/Head and Neck Surgery and Department of Biomedical Engineering, Columbia University, New York, New York 10032, USA

(Received 1 June 2015; revised 5 September 2015; accepted 10 October 2015; published online 12 November 2015)

The classical picture of middle ear (ME) transmission has the tympanic membrane (TM) as a piston and the ME cavity as a vacuum. In reality, the TM moves in a complex multiphasic pattern and substantial pressure is radiated into the ME cavity by the motion of the TM. This study explores ME transmission with a simple model, using a tube terminated with a plastic membrane. Membrane motion was measured with a laser interferometer and pressure on both sides of the membrane with micro-sensors that could be positioned close to the membrane without disturbance. A finite element model of the system explored the experimental results. Both experimental and theoretical results show resonances that are in some cases primarily acoustical or mechanical and sometimes produced by coupled acousto-mechanics. The largest membrane motions were a result of the membrane's mechanical resonances. At these resonant frequencies, sound transmission through the system was larger with the membrane in place than it was when the membrane was absent.
 [http://dx.doi.org/10.1121/1.4934515]

[CAS] Pages: 2972–2985

I. INTRODUCTION

The tympanic membrane (TM) is a nearly transparent membrane, 10 μm thick in gerbil, 100 μm thick in human, that moves in a complex multiphasic motion in response to a sound stimulus (e.g., Khanna and Tonndorf, 1972; Cheng *et al.*, 2013). Building on these observations, some current models have the middle ear (TM + ossicles) operating as a series of mistuned resonances (Funnell and Laszlo, 1978; Funnell *et al.*, 1987; Fay *et al.*, 2006). Another consideration is that the TM's movement in response to sound will produce pressure within the middle ear (ME) cavity. In an abstract analytical model, Rabbitt (1990) showed that the TM radiated considerable sound pressure into the ME cavity, which reflected and drove the TM from the ME side. We recently explored these ideas with pressure measurements within the ear canal (EC) and the ME cavity in gerbil (Bergevin and Olson, 2014), and those observations reaffirmed the TM's multiphasic motion and confirmed the prediction that TM motion would lead to significant pressure and a resultant standing-wave pressure field within the ME cavity.

Two components of the ME system are particularly significant to sound transmission and can be simplified to understand aspects of the basic behavior. In an abstract limit, the EC can be modeled as a tube and the TM as a membrane. This study focused on these two aspects of the mechanics, employing a simple system of a tube terminated with a flat plastic membrane. The membrane dimensions were similar to those of the gerbil TM the diameter of which is ~4 mm with ~10 μm thickness (Kuypers *et al.*, 2005). Our tube length of 43 mm was not a model of the gerbil EC, which is much shorter. This length is similar to the EC length in human and provided richer acoustics for our study. Thus our study is of the acousto-mechanics of a system with components like those of the ME. Pressure was measured both near and relatively far from the membrane with a micro-pressure sensor and membrane velocity was measured with a laser interferometer. A finite element model (FEM) of the system was developed, and its predictions were used to interpret the experimental results. Many previous studies have employed pressure measurements within the EC and acoustic models with various objectives: for example, to quantify ME transmission, to understand transmission of otoacoustic emissions, and to diagnose middle ear pathology (e.g., Keefe *et al.*, 1993; Ravicz *et al.*, 2007; Puria and Allen, 1998; Stinson, 1985). The present model is more abstract than these, and its strength lies in the precise matching between experimental and modeling results. In addition to a tube + membrane system, four related and even simpler systems were analyzed to evaluate effects of the different sub-components.

II. METHODS

A. Experimental setup

The physical tube and membrane system was made by gently stretching plastic wrap over the end of a glass tube of inner diameter 5.8 mm and length 43 mm (Fig. 1). Household plastic wrap is composed of low density polyethylene (LDPE) the mechanical properties of which are: density 940 kg/m^3 and Young's modulus within a range including the value we use, 250 MPa (Sakurada *et al.*, 1981). The thickness of the

a)Also at Biomedical Engineering, Columbia University, New York, NY 10032. Electronic mail: eao2004@columbia.edu

membrane is 0.013 mm according to on-line data provided by Dow, a manufacturer of household plastic wrap. This was confirmed by using the measured mass of a piece of plastic wrap and the density of LDPE to calculate thickness. A thin film of gold (~50 nm) was evaporated onto the membrane to make it reflective for laser-interferometric motion measurements.

Pressure was measured with fiber-optic pressure sensors of inner/outer diameter 75/125 μm that were constructed in the lab (Olson, 1998). The sensor was held in a motorized micromanipulator (Marzhauser) with 1 μm step size resolution. Pressure was measured along the axis of the tube with a 5 mm step size, starting at a location ~10 mm from the inner surface of the membrane. Pressure was also measured outside the tube end (the end with the membrane), along the tube axis. Outside the tube, the measurement spacing was relatively dense, 90–100 μm close to the outer surface of the membrane where pressure varied rapidly. Based on FEM results, the effect of the sensor on the acoustic field was not significant. The velocity of the membrane in the direction perpendicular to its surface was measured with a heterodyne interferometer that was coupled to a translation and rotation stage (Khanna *et al.*, 1996). Stimulus generation and data acquisition were performed with a Tucker Davis Technologies System III and MATLAB. The stimulus pressure was provided by a Radio Shack tweeter terminated by a speaker-tube. The speaker-tube was positioned ~1 cm from the membrane at an angle of 45°. A reference pressure was measured halfway between the sound source and the membrane with a probe-tube microphone. The sound pressure level was ~1 Pa at the reference. Data analysis was performed via FFT using MATLAB.

B. Numerical modeling

We built and analyzed several related FEMs. The main model corresponds to the experiment that was performed on a tube, terminated on one end with a flexible membrane [Figs. 2(a) and 3]. Considering its mechanical geometry, with a very small thickness (13 μm) compared with the radius (2.9 mm), the termination can be described as a membrane. This is reinforced by the small pre-stress that was applied when constructing the experimental system. Because of the small displacement magnitude, the stresses and motions were linear.

In addition to the tube and membrane, four related systems were analyzed to evaluate effects of the different sub-components of the total system. The tube was calculated without the membrane in two configurations: both sides open [open-open, Fig. 2(b)] and with the side corresponding to the membrane closed [open-closed, Fig. 2(c)]. The membrane alone was analyzed by modeling the membrane within a baffle [baffle membrane, Fig. 2(d)]. This configuration was also explored experimentally but with a different membrane thickness in a previous report (Gonzalez-Herrera *et al.*, 2013). We also modeled the baffle without the membrane [hole baffle, Fig. 2(e)] to better understand the behavior of the membrane and baffle at a frequency for which the membrane had a mechanical resonance.

Most of the numerical aspects of the models are common to all of the configurations. The following description refers to the main model (tube and membrane). The ANSYS program was used to model and calculate the problem. The numerical model comprised a solid domain corresponding to the membrane and a fluid domain for the surrounding air. The domains were in contact at the membrane faces where a coupled fluid-structure problem was implemented. The tube and the baffle were taken as perfectly rigid and with zero thickness. The fluid was limited to the volume within a sphere the surface of which was represented by a specific ANSYS element, (FLUID130). The size of the sphere was taken as 7 cm in diameter for which reflections were effectively eliminated. The sound source was represented as a cylinder with dimensions equal to that of the tube that terminated the speaker. Sound pressure was applied as a unitary load (1 Pa) (Figs. 1 and 3) at an approximate distance of 1 cm and 45°, corresponding to the actual experiment.

Due to its symmetry, only half the problem was modeled and calculated with symmetry boundary conditions applied on the midplane of the sphere. Details of the model

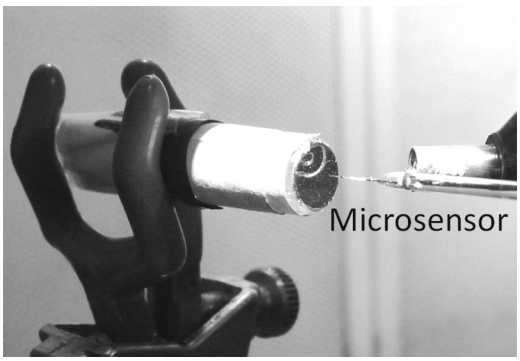

FIG. 1. Setup for pressure measurement.

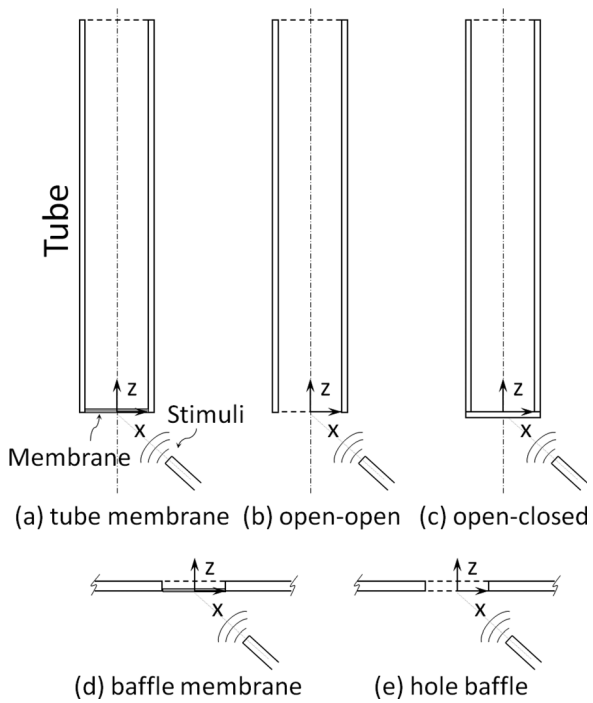

FIG. 2. Problems solved by FEM: (a) tube-membrane, (b) open-open, (c) open-closed, (d) baffle-membrane, and (e) hole-baffle.

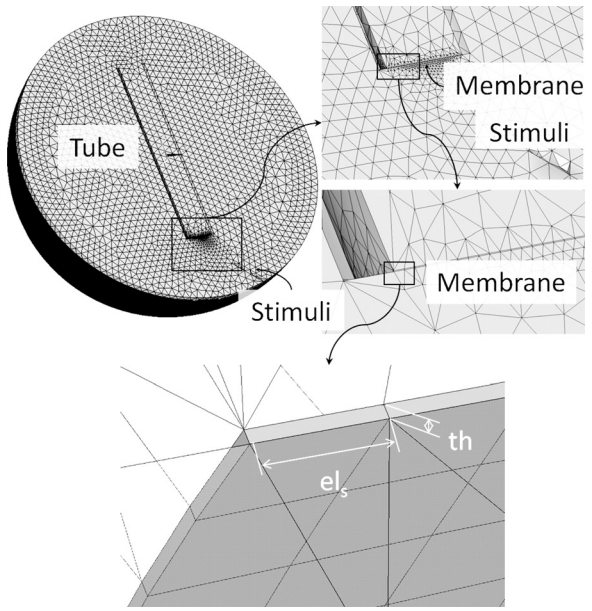

FIG. 3. FEM tube and membrane problem and membrane mesh size detail.

mesh are shown for the different geometries in Fig. 3. A parametric geometric model was developed with the ANSYS program and then meshed.

The fluid was represented with acoustic elements (FLUID30). Fluid30 behaves according to the acoustic wave equation assuming an inviscid fluid with uniform mean density and pressure. It is able to model the fluid medium and the interaction with an interface in fluid/structure problems. In this case, it takes into account the coupling of acoustic pressure and structural motion at the interface. It has been used in its tetrahedral form, with four nodes and linear shape function. Each node has four degrees of freedom: translations in *x, y*, and *z* directions and pressure. Translational degrees of freedom are only used at nodes on the interface, reducing the computational cost. The elements have the capability to include damping of sound-absorbing material at the interface. The speed of sound was 343 m/s and air density was 1.21 kg/m^3. The acoustic absorption coefficient for the tube surface was 0.003 and for the membrane was 0.01. These values were found by fitting model predictions with experimental results. The maximum element size was established to capture the wave effects over the frequency range of interest. The size of the elements in the fluid domain was limited to at most 1.7 mm in order that the wavelength of the maximum frequency of 20 kHz (17.1 mm) was meshed with at least 10 elements. The element size was smaller close to the membrane. The minimum element size was constrained by the size of the solid elements used to mesh the membrane as will be detailed in the following text.

The membrane was represented by solid elements (SOLID185). SOLID185 is a 3D structural element that can be used in prism, tetrahedral, and pyramid forms. In its prism form, it is defined by eight nodes with 3 degrees of freedom at each node: translations in *x, y*, and *z* directions. In this particular work, it has been used with enhanced strain formulation (as will be justified later), where the common isoparametric formulation with linear shape function is complemented with additional internal degrees of freedom to overcome the shear-locking problem that is present in bending-dominated problems. In addition to the physical properties of the membrane material (LDPE) described in the preceding text, the Poisson's ratio was taken as 0.49 and damping was included via a material coefficient damping ratio, $\xi = 0.001$ (0.1%). This parameter was initially estimated at a slightly higher value and updated to this value based on the numerical results.

The membrane geometry posed a difficulty. The thickness dimension was much smaller than the diameter: the diameter/thickness ratio was 446. Additionally, the mechanical response is dominated by bending behavior that is usually difficult to model with solid elements, which are affected by the shear-locking problem of structural mechanics calculations. To avoid a very fine mesh containing an unacceptably large number of elements, hexahedral elements with enhanced strain formulation (we call them "Hexa ESF") were used. This element introduces 13 internal degrees of freedom to overcome shear-locking (Simo and Rifai, 1990; Simo *et al.*, 1993; Andelfinger and Ramm, 1993). The efficiency of this formulation was evaluated with a mesh convergence study to establish the maximum element size at the membrane that was acceptable to obtain valid results. The membrane was meshed with an automatic routine controlled by a parameter corresponding to the maximum element length permitted (el_s). Finally the mesh obtained was like that shown in Fig. 3. Due to the small thickness of the membrane ($th = 13\ \mu m$), the ratio el_s/th must be limited to values below 10 to obtain valid results.

The convergence analysis was done based on a modal analysis of several FE models of the membrane with the same dimension and material but different element size. The first, fourth, and ninth natural frequencies, corresponding to the unimodal [classical membrane mode (0, 1)] and "sombrero" [(0, 2), (0, 3)] shaped modes were considered to evaluate the convergence. (On the top of Fig. 12 we show the patterns of several of the natural modes.) These classical circular-membrane modes are found in books on acoustics and musical acoustics (e.g., Hall, 1993). The convergence rate was different for the different modes. As expected, convergence was reached with a larger mesh dimension at the lower frequencies where the shape was simpler, and so there was less bending. The target values were calculated with a simple shell model. Results are plotted in Fig. 4 for three different types of FE modeling, first the target result with shell elements ("shell") and then with hexahedral solid elements in one case with enhanced strain formulation ("Hexa ESF") and the other with a usual formulation ("Hexa"). Only one layer of elements was used for the thickness in all cases.

The convergence was studied in terms of the element shape ratio (el_s/th) and in terms of the number of divisions of the radius, (radius/el_s), and for the purposes of illustration, the results of the second study are shown in Fig. 4. The convergence of the shell model is the best and is good even with a very low number of elements. However, this type of element does not allow fluid-structure interaction coupling on both sides of the membrane and cannot be used. Focusing on

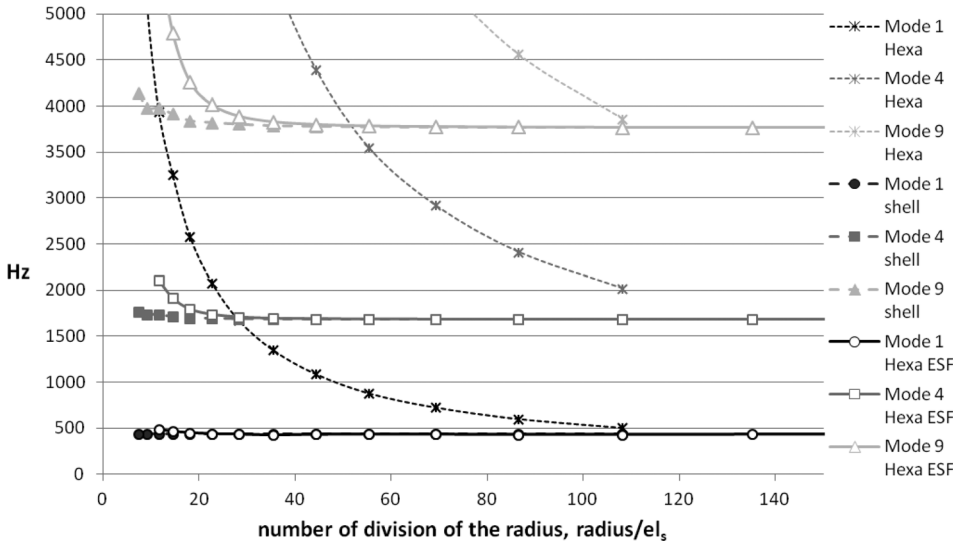

FIG. 4. Mesh size convergence study. Results from a standard hexagonal element model (Hexa) and a model that incorporates an enhanced strain formulation (Hexa ESF) are compared with a shell model, which provided target values. The calculation of natural frequencies for modes 1, 4, and 9 with different mesh sizes are used as reference for the study. In the figure the convergence is studied in terms of the ratio of the radius of the membrane to the element length.

the hexahedral elements we can see that the convergence is good with the Hexa ESF element and poor with the common (Hexa) formulation. The common Hexa formulation case is not acceptable from a computational cost point of view because a very high number of elements would be necessary to obtain the correct results (element length <100 divisions of the radius). The use of Hexa ESF elements provides a good balance between accuracy and element size. An element size of 130 μm, which is 10 times the thickness and 22 divisions of the radius, was considered acceptable for this work, which focused on the lower natural frequencies of the membrane. (We will return to this when discussing Fig. 12.) In summary, the membrane was meshed with a maximum element size of 130 μm. Regarding the fluid elements, close to the membrane the mesh size was 130 μm, and it gradually increased to a maximum size of 1.7 mm far from the membrane.

During the coupling of the plastic wrap to the tube, a small tension was applied to the film to avoid wrinkles and obtain a planar shape. Experimentally, the degree of prestraining was difficult to measure or estimate and, at the same time, significant to the dynamic response of the membrane. Thus this parameter was necessarily evaluated based on the experimental results. In our numerical model, the prestrain was introduced as an additional load step in which the perimeter of the circular membrane was subjected to an imposed radial displacement u_{rad}. As a consequence, the membrane acquired a strain field where the two principal strains are $e_{11} = e_{22}$ in the plane of the membrane (and $e_{33} = -2e_{11}$). This homogeneous situation is ideal, and the actual strain was not perfectly homogeneous. Nevertheless the homogenous approximation was useful to understand and interpret the results. The influence of the pre-strain (in terms of e_{11}, e_{22}, or u_{rad}) on the dynamic response of the membrane (in a vacuum) is illustrated in Fig. 5 where the first six natural frequencies are plotted at different levels of pre-strain. Pre-strain increases the stiffness of the system and so shifted the natural frequencies upward. We determined the value of the pre-strain parameter to use in the model based on the value of the second natural mode of the experimental results. The membrane's first natural mode frequency was not useful for this purpose because it was close to an acoustic tube resonance and also because the first resonant frequency of the membrane is a uniphasic motion, and the fluid mass of the air shifts the resonant frequency downward significantly from the theoretical value of a membrane in a vacuum. Accepting that the rest of the mechanical parameters of the model (material properties and dimensions) have been estimated or measured with reasonable accuracy, prestrain was the only free parameter needed to obtain the corresponding second natural mode frequency. In our case, frequency = 7.6 kHz (m2 in Table I), and the pre-strain is found to be $\varepsilon_{11} = 0.00275$, which corresponds to a very small radial displacement of $u_{rad} = 8$ μm.

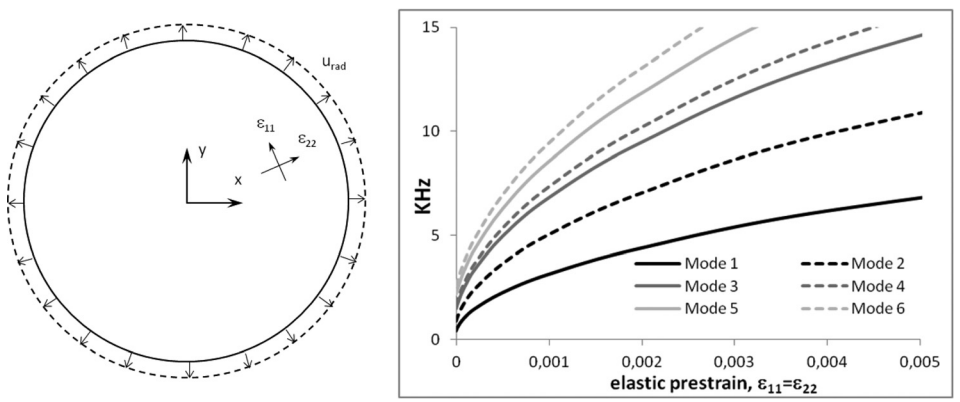

FIG. 5. The effect of membrane prestrain on the natural frequencies of the membrane. The first six modes are shown. The mode 2 curve was used with experimental results to determine the pre-strain value for the model.

TABLE I. Resonance frequencies (in kHz) of membrane and tubes considered as separate systems and as combined system in final row. For the different subsystems (membrane, open-closed tube, and open-open tube), the resonance frequencies were affected slightly by the way in which they were calculated. For the membrane, these are the shell and solid-element FEM with the analytical result for the frequency ratios of a circular membrane included for comparison (to use that row multiply the ratio by the m1 value). For the tubes, the resonances were first calculated with the classical formulas relating to tube length, L, and then including the effective length that accounts for pressure spreading outside the tube, where $L_{\text{eff}} = L + 0.61r$ where r is the radius, and finally with the FEM. The m#, tc#, to#, and tm# labeling correspond to the membrane, the closed-open tube, the open-open tube and the tube + membrane systems.

System	Resonant frequencies in kHz and their labels								
Membrane	**m1**	**m2**	**m3**	**m4**	**m5**	**m6**	**m7**	**m8**	**m9**
Shell model	4.7	7.6	10.2	11	12.7	14	15.2	16.9	17.5
Solid element	4.7	7.6	10.4	11.4	13.3	14.6	16	17.8	18.5
Classical membrane mode	(0,1)	(1,1)	(2,1)	(0,2)	(3,1)	(1,2)	(4,1)	(2,2)	(0,3)
Classical freq. ratio (m#/m1, unitless)	1	1.59	2.14	2.30	2.65	2.92	3.15	3.50	3.60
Tube open-closed	**tc1**	**tc2**	**tc3**	**tc4**	**tc5**				
Simple classical	2	6	10	14	18				
$L + 0.61r$	1.9	5.7	9.6	13.4	17.2				
FEM	1.9	5.8	9.7	13.6	17.5				
Tube open-open	**to1**	**to2**	**to3**	**to4**	**to5**				
Simple classical	4	8	12	16	20				
$L + 0.61r$	3.8	7.6	11.5	15.3	19.1				
FEM	3.7	7.5	11.2	14.7	18.8				
Tube + membrane	**tm1**	**tm2**	**tm3**	**tm4**	**tm5**	**tm6**	**tm7**		
FEM	1.6	4.2	6.7	9.8	11.4	14	18.1		

III. RESULTS

A. General description

Sound pressure is plotted in Figs. 6 and 7 for a general overview of the response of the different systems. The variable plotted is sound pressure in decibels where 0 dB corresponds to the sound pressure at the sound source. A double spatial and frequency domain plot is used. Spatial z axis corresponds to the central axis of the tube [$x = y = 0$, see Fig. 2(a)]. When it is present, the membrane is placed at the coordinate $z = 0$. The plot ranges from $z = -10$ mm, which is in front of the membrane and close to the speaker, to 7 mm outside the far end of the tube ($z = 50$ mm). The numerical result for the tube-membrane system is plotted in Fig. 6(a) and the corresponding experimental result in Fig. 6(b). (Due to the risk of breaking the membrane during the experiment, there is a gap at the interior of the tube because sound pressure was only measured up to 10 mm from the membrane.) Two key aspects can be highlighted. On the one hand, peaks are present at certain frequencies in the area close to the membrane at ~4, 7, and 11 kHz. These correspond to mechanical resonances of the membrane. The resonant frequencies corresponding to these modes are the m1–m9 values in Table I. On the other hand, inside the tube, acoustic resonances related to the tube length are observed. These two different effects are present in the same range of frequencies; their responses are coupled and can be difficult to distinguish.

To better understand the behavior of the system, four additional systems were studied numerically. These are the models sketched in Fig. 2. In Fig. 7, the spatial distribution of pressure along the axis is plotted for a range of frequencies from 0 to 15 kHz. The scale is the same for all the figures and ranges from −80 to 10 dB. If we make a section of these figures for a specific location (z) inside the tube, we obtain a frequency response function, FRF [Fig. 8(a)]. Similarly, if we make a section for a specific frequency, we see the sound pressure distribution along the axis inside and outside the tube (Fig. 9).

The effect of the tube can be understood by considering two limiting cases. In the limit that the membrane is stiff and does not let the sound go through, the system can be considered as a tube with a closed end. In this case, sound pressure within the tube enters it from the far, open end of the tube [Figs. 2(c) and 7(c), open-closed tube]. On the other hand, in the limit that the membrane transmits the sound freely, the tube would behave as an open-ended tube [Figs. 2(b) and 7(a), open-open]. The actual behavior is between these two situations, with additional structure due to the membrane's dynamics. The membrane response was also calculated with the presence of a baffle without a tube [Figs. 2(d) and 7(d), baffle membrane]. In this case, the membrane is excited on one side, transmitting sound to the other. The case of the hole in baffle without the membrane [Fig. 2(e)] was also calculated in order to uncouple the influences of the hole and the membrane. This result is plotted in Fig. 7(b) (hole baffle).

The main resonance frequencies of each separate system are displayed in Table I. The membrane resonance frequencies and mode shapes were calculated by means of a modal analysis of a FEM of the membrane including the pre-strain (pre-strain $\varepsilon_{11} = \varepsilon_{22} = 0.00275$). The sequence of mechanical resonance frequencies are approximately as expected based on the Bessel function analytical result for a membrane, also shown in the Table (Hall, 1993). The tube resonance frequencies were obtained with the classical expression in terms of the sound-speed, c, and tube-length, L. For the open-open case the tube resonant frequencies are $f_n = nc/2L$ $n = 1,\ldots$, corresponding to to1, to2,… in Table I and for the open-closed case they are $f_n = c(2n-1)/4L$ $n = 1,\ldots$,

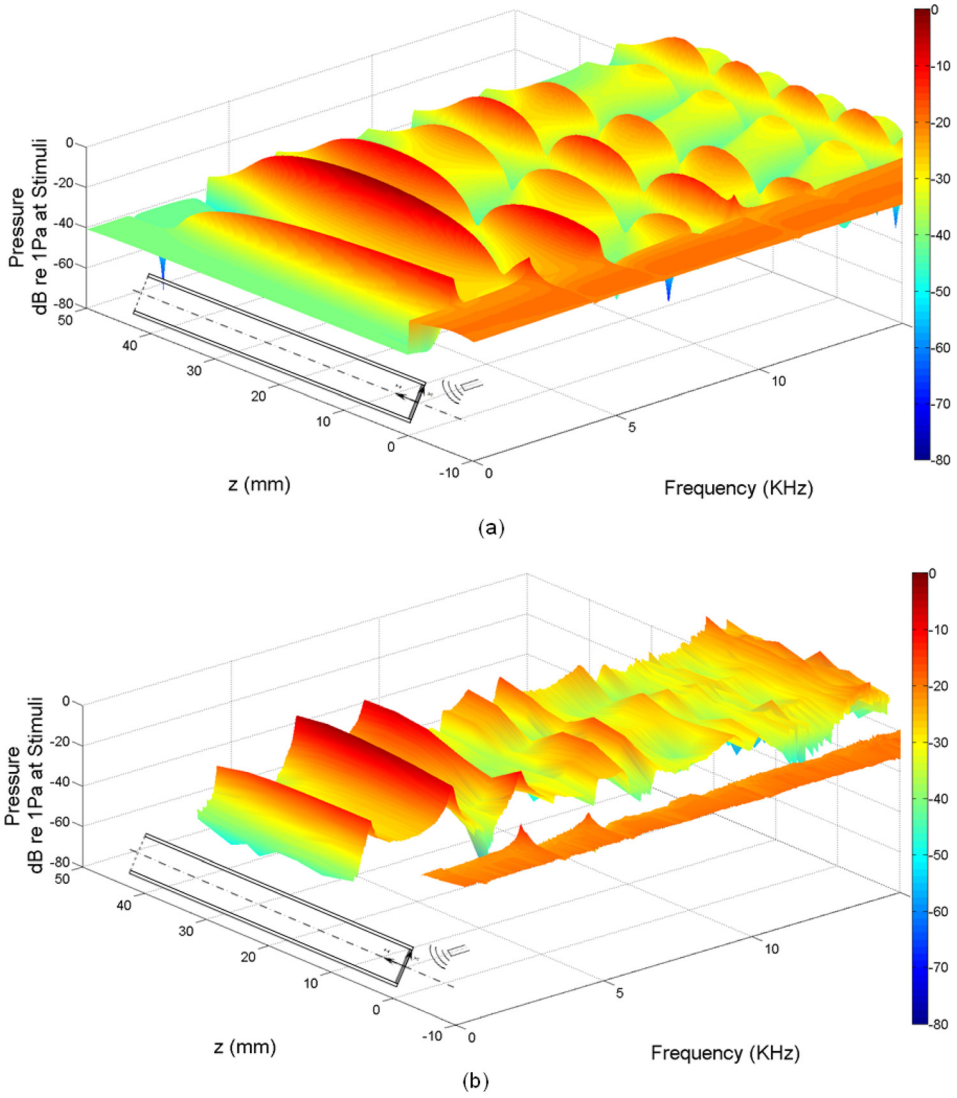

FIG. 6. (Color online) Pressure field along the axis of the tube of the tube + membrane system. (a) Numerical results. (b) Experimental results. The gap in (b) is the region just behind the membrane in which pressure was not measured.

corresponding to tc1, tc2,… in Table I. These values were not calculated with the "effective length" that takes into account the pressure field extending from the open tube end, and a correction using an effective length of $L + 0.61r$ (r the tube radius) introduces small downward shifts in the predicted tube resonance frequencies (also shown in Table I). The length-corrected predictions of acoustic resonance frequencies are in better accordance with the frequencies obtained with the FEM. For simplicity in the discussion in the following text, we refer to the whole number (uncorrected for effective length) frequencies (2, 4, 6 kHz…) as the acoustic resonance frequencies of the tube.

An important feature of the tabulated resonant frequencies is that many are very close, as in the case of m1 and to1. In both the FEM theory and experiment of the tube-membrane system, these nearby resonances combine. Going back to the tube-membrane system of Figs. 7(e) and 7(f), we observe how the total system behaves as a combination of the simpler models. We can identify maximum responses at different frequencies and these are tabulated in Table I (tm1, tm2….). Those maxima are related to the sound pressure gain inside the tube. Comparing Figs. 7(a), 7(c), and 7(e), the first (tm1) and second (tm2) frequencies of Fig. 7(e) are very similar to the first resonance of a closed/open and open/open ended tube, respectively. The third and following frequencies lay at intermediate positions between the simple open/open and open/closed tubes in a more complex pattern. This can be easily visualized in Fig. 8(a) where the FRF for a position inside the tube is plotted ($z = 11$ mm from the membrane). Numerical and experimental results for the tube-membrane system agree reasonably well. Numerical predictions for the simple systems are included in Fig. 8(a) and reaffirm that the first and second peaks of the tube-membrane system are close to the open-closed and open-open model first peaks. The velocity at the center of the membrane is plotted in Fig. 8(b). Comparing the membrane-tube result with that of the baffle-membrane model, we see that the second tube-membrane peak, in addition to being close to the open-open acoustic resonance, is also nearly coincident with the 11 kHz m4 resonance of the membrane.

The effect of the membrane-baffle, or hole-baffle [as illustrated in Figs. 7(b) and 7(d)] is most significant very close to the hole (within ~2 mm) and at the membrane's mechanical resonant frequencies. Responses at those frequencies are explored in Figs. 9(d) and 9(f) and will be discussed in the following text.

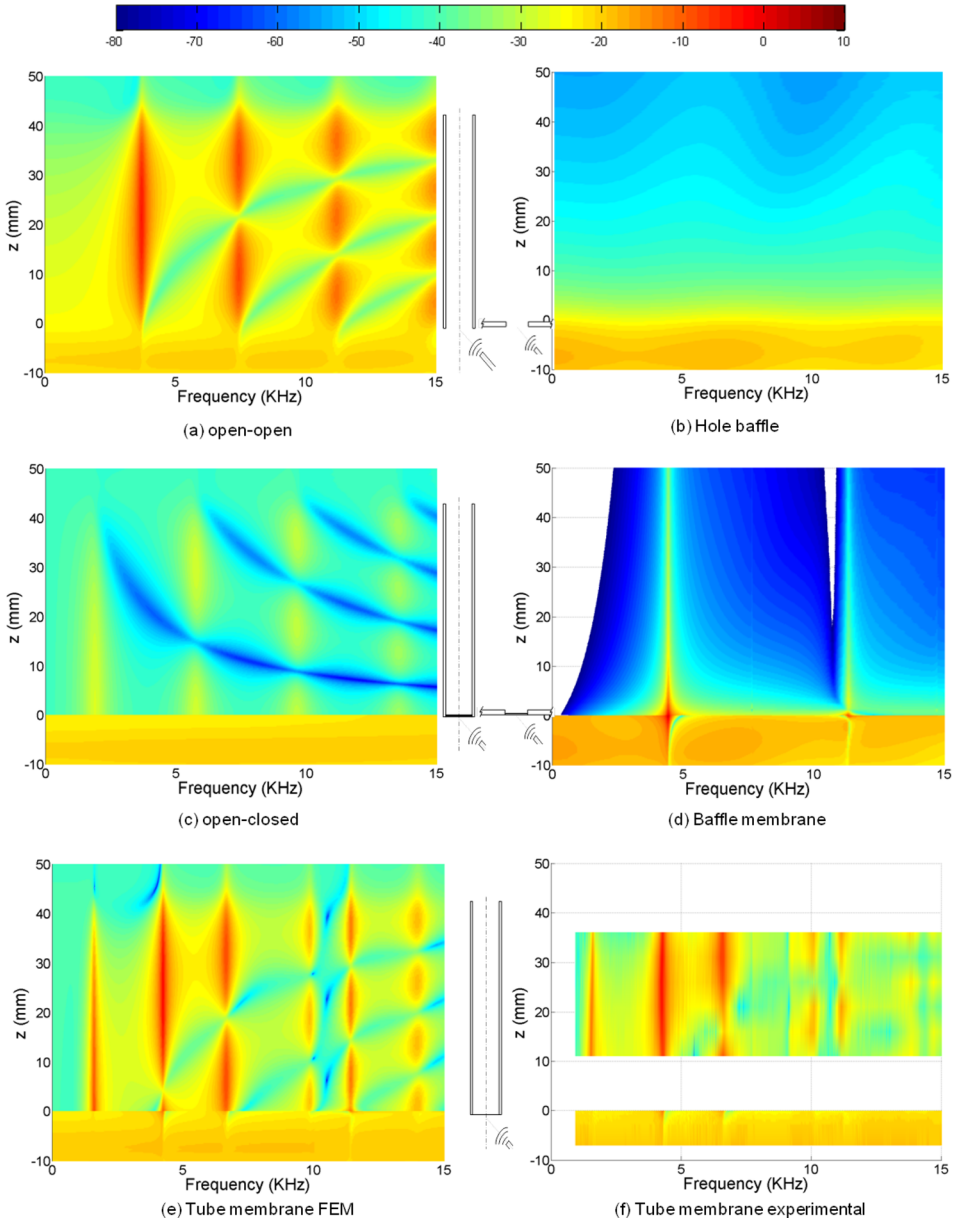

FIG. 7. (Color online) (a)—(e) Numerical results, pressure field along the z axis indicated in the central sketches (along the axis of the tube or perpendicular to the baffle, passing through the center of the hole). Several different models are considered, as indicated in the captions in the figure. (f) Experimental results of the tube-membrane experiment.

B. Representative frequency ranges

An effective way to understand the behavior of the system is to inspect the response at specific frequencies where particular aspects of the mechanics are dominant. To this end, in Fig. 9, sound pressure along the z axis ($x = y = 0$) is plotted at selected frequencies. Numerical results for the tube-membrane and more basic systems and experimental results for the tube-membrane are shown. The experimental results are the gray solid lines with dots noting the measurement locations within the tube; outside the tube the measurement points were relatively dense and not indicated individually. It is notable that in all frequency ranges, there is good correspondence between experimental and numerical tube-membrane results.

Range 0–1 kHz: This range of frequencies represents the pseudo-static response of the system [Fig. 9(a), at 1 kHz]. The tube-membrane response is very similar to the open-closed response——thus the pressure inside the tube is primarily due to the sound entering from the open, back side of the tube. There is a small displacement of the membrane proportional to the sound pressure applied, but there is no pressure gain due to any dynamic effect. Pressure drops across the membrane and the closed tube are both ∼15 dB. In the case of the baffle-membrane, the drop across the membrane is much larger because there is no back route for the sound.

1.58 kHz [Fig. 9(b)]: At this frequency [corresponding to the first peak in Fig. 8(a), tm1], the effect of a quarter-wave acoustic resonance appears. The resonance frequency is lower than the classical quarter-wave resonance frequency (2 kHz), and it is shifted downward both by the movement of the membrane (compared with the truly closed-ended tube) and also because the effective length of the open tube is slightly longer than the physical length (see Table I). The tube resonance produces 30–40 dB pressure gain at the membrane as measured from the back side of the tube, but this pressure is not

transmitted by the membrane to the exterior ($z < 0$), where the pressure in the tube-membrane condition is quite similar to the pressure in the other systems despite the large differences in pressures within the tube ($z > 0$) across systems. It is notable that because of the tube's acoustic resonance, the sound pressure within the tube of the tube-membrane system is much larger than it is on the exterior side of the membrane, close to the sound source.

3 kHz [Fig. 9(c)]: At this frequency, the effects of the tube resonances tm1 and tm2 are observed in the sound pressure gain within the tube. The frequency is not close to a membrane mechanical resonance and the membrane has only a small displacement. The pressure at the external side of the membrane is not much affected by the internal pressure——as in the cases of Figs. 9(a) and 9(b), the external pressure is quite similar across systems, while the internal pressure is quite different.

4.24 kHz [Fig. 9(d)]: Two resonance effects are present in the range of 4–4.5 kHz. This range is approaching the membrane's first mechanical resonant frequency, predicted to occur at ~4.7 kHz. The strong effect of this resonance is shifted downward in frequency due to air mass adding to the mass of the membrane, as will be clearly seen in Fig. 11. The open-open half-wave tube resonance at 4 kHz also influences the response. The baffle-membrane and open-open tube FRFs in Figs. 8(a) and 8(b) underscore these contributions to the 4.24 kHz response observed in Fig. 9(d). It is notable that the effects of the mechanical + acoustical resonances are most prominent at a different frequency (4.24 kHz) than either of the two resonances considered separately. There is a maximum within the tube that is similar to the system with both open ends; this is attributable to the open-open tube acoustical resonance. In addition, there is a substantial pressure increase at locations within ~2 mm of the membrane, both internal and external to the tube. This is due to the mechanical resonance of the membrane (with surrounding air adding mass), and the resulting membrane motion, which essentially becomes a pressure source. This behavior of the mechanically resonant membrane as a pressure source is particularly clear when comparing the baffle-membrane and hole-baffle curves. The baffle-membrane curve is displaced upward significantly compared to the hole-baffle curve with a 3 dB increase persisting to large z values——thus the presence of the membrane enhances the sound transmission through the hole.

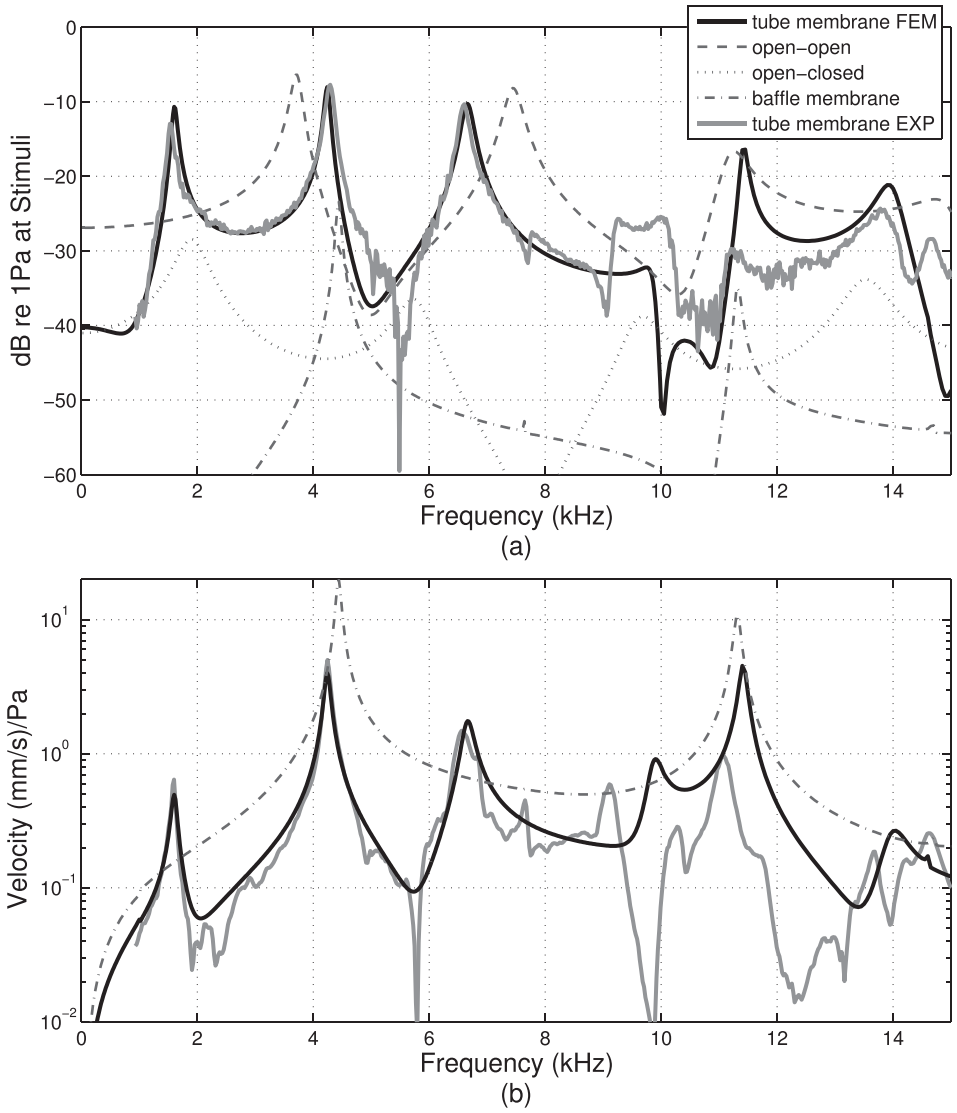

FIG. 8. (a) Pressure frequency response function at one location along the axis of the tube, 11 mm behind the membrane (or behind the baffle hole). Experimental and modeling results are shown. (b) Corresponding velocity of the membrane at the center of the membrane.

6.6 kHz [Fig. 9(e)]: At this frequency, several resonant effects are present: open-closed tube (6 kHz), open-open tube (8 kHz), and the second natural frequency of the membrane (7.6 kHz). The resonance of the membrane it is not apparent in this plot——there is not an enhanced pressure close to the membrane as in Fig. 11(d)——because the middle of the membrane is a node in the second natural mode, m2 = (1,1) (see mode sketches at top of Fig. 12). Likely because of the antisymmetric motion, the membrane does not act as an effective pressure source and the sound transmission of the baffle-hole system exceeds that of the baffle-membrane system all along the z axis within the tube.

11.3 kHz [Fig. 9(f)] and higher frequencies: In this range of frequency and higher, the membrane vibrates in a more complex pattern. Inside the tube the corresponding resonant effects can be observed. The membrane mode m4 = (0, 2) "sombrero" mechanical resonance is also apparent and is particularly clear when considering the curve corresponding to the baffle-membrane system. As in Fig. 9(d), the presence of the membrane in the membrane-baffle case boosts sound transmission compared to the baffle-hole case, here by an even larger amount, ~6.5 dB. Thus the membrane's mechanical resonances act as a mechano-acoustical filter; the system operates as a relatively open gate for sound transmission at some frequencies and a relatively closed gate at other frequencies.

C. Mechanical impedance

In the final results section, we concentrate on the tube + membrane system, and the paper will end with one comparative figure from the baffle + membrane system.

In Fig. 10, experimental and numerical pressure and velocity variables for the center of the membrane are plotted. Pressure outside and inside the tube (at 10 μm distance) and the velocity at the center are shown in magnitude and phase. Experimental results are also plotted when they are available. Figure 10 focused on the range of frequencies from 4 to 5 kHz, which we expected to contain the first mechanical resonant mode of the membrane. The peak in the velocity graph [Fig. 10(c)] shows the presence of a resonance, but because the pressure adjacent to the membrane [Fig. 10(a)] also exhibits a peak, it is not possible to use the velocity peak to pinpoint the resonant frequency of the membrane alone (its purely mechanical resonance). Pin, Pout, and velocity all have different but similar peak frequencies.

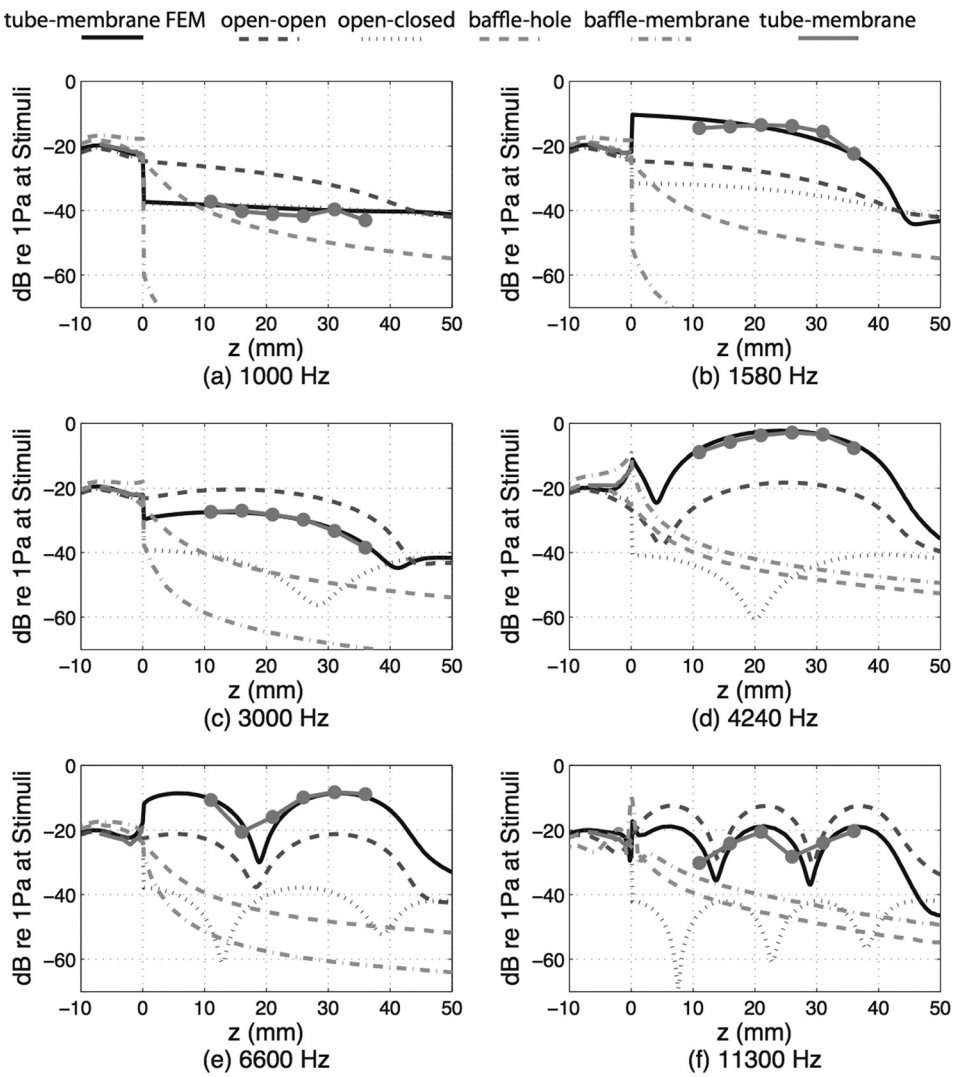

FIG. 9. Pressure field along the axis of the tube or the axis perpendicular to the baffle. The different panels show different frequencies of interest based on previous results. The experimental results are shown in the gray solid lines with the measurement locations within the tube noted with dots. Adjacent to the membrane outside the tube the measurement spacing was much greater, resulting in a smoother curve and individual points are not indicated.

Pin and pout follow alternate trends below and above the peaks. At 4 kHz, the membrane acts as a relatively stiff barrier [see also the velocity plot of Fig. 10(c)]. Pressure is higher outside than inside. As frequency increases and we approach the peak frequency, the pressure increases on both sides and the difference between them is reduced. When the outside pressure (pout FEM) is at maximum, inside (pin FEM) it keeps growing. As the frequency increases, the outside pressure drops more quickly than the inside pressure, and has a local minimum at ∼4.4 kHz.

The impedance of the membrane alone, $Z = \Delta P/\text{velocity}$, was found using the pressure and velocity values at the membrane center. First we used the FEM data to calculate the pressure difference across the membrane ($\Delta P = $ pout - pin, the complex difference). The result is shown in Fig. 10(a) (dotted line). Again a maximum appears basically coincident with the maximum of the velocity. The impedance is shown in Figs. 10(e) and 10(f). The magnitude is trending downward gradually, and the phase is close to −90°, so through this frequency range, the membrane alone is stiffness dominated. It is the membrane + airmass system that gives rise to the pressure and velocity response peaks at ∼4.2 kHz, and the ratio corresponding to the impedance of the membrane alone is not peaked. To provide a reference value for the properties used in this work, the specific acoustic impedance of air is $Z_{air} = 415$ Pa/(m/s). The membrane-alone impedance resonance is slightly higher than 5 kHz (as will be shown in Fig. 11) and did not appear within the 4–5 kHz frequency range.

In Fig. 10 we showed pressure and velocity values at the center of the membrane, and calculated Z based on these values. However, because our system is distributed, a better understanding can be obtained if we study the spatial distribution of Z. In Fig. 11, we extend the frequency range to 6 kHz and show the responses at the three locations on the membrane indicated in the inset diagram. In Fig. 11, the resonant mechanical impedance of the membrane alone is apparent. We had expected the first membrane resonance to occur at ∼4.7 kHz (see Table I), but this was based on the theoretical resonance frequencies of a membrane and depended in part on the pre-stress parameter. We see in Fig. 11 that when considering the center of the membrane, the membrane-alone resonance was shifted slightly higher than this prediction. While Pout, Pin, and velocity are all smoothly and gradually varying with frequency, with a single prominent peak, pout and pin can become nearly equal in magnitude and phase at a frequency that depends on the particular location on the membrane. In such cases, the pressure difference exhibits a sharp notch. The notch is particularly steep for the center position at ∼5.3 kHz. Because this is a frequency well above the peak in velocity, when the ratio is taken the membrane-alone impedance has a steep minimum at this frequency as well, and the phase undergoes the expected transition from −90° (stiffness dominated) to +90° (mass dominated) [Fig. 11(J)]. At the position closer to the sound source, the impedance magnitude goes through a more gradual minimum at 4.7 kHz, and at the same frequency, the phase goes from −90° (stiffness dominated) to −270° (mass dominated), but the direction of the transition is reversed, which can be traced back to the specifics of the Pout, Pin magnitudes and phases. At the position furthest from the sound source, the pressure difference goes through a very mild minimum accompanied by a mild phase variation. Thus the concept of point mechanical impedance is only roughly

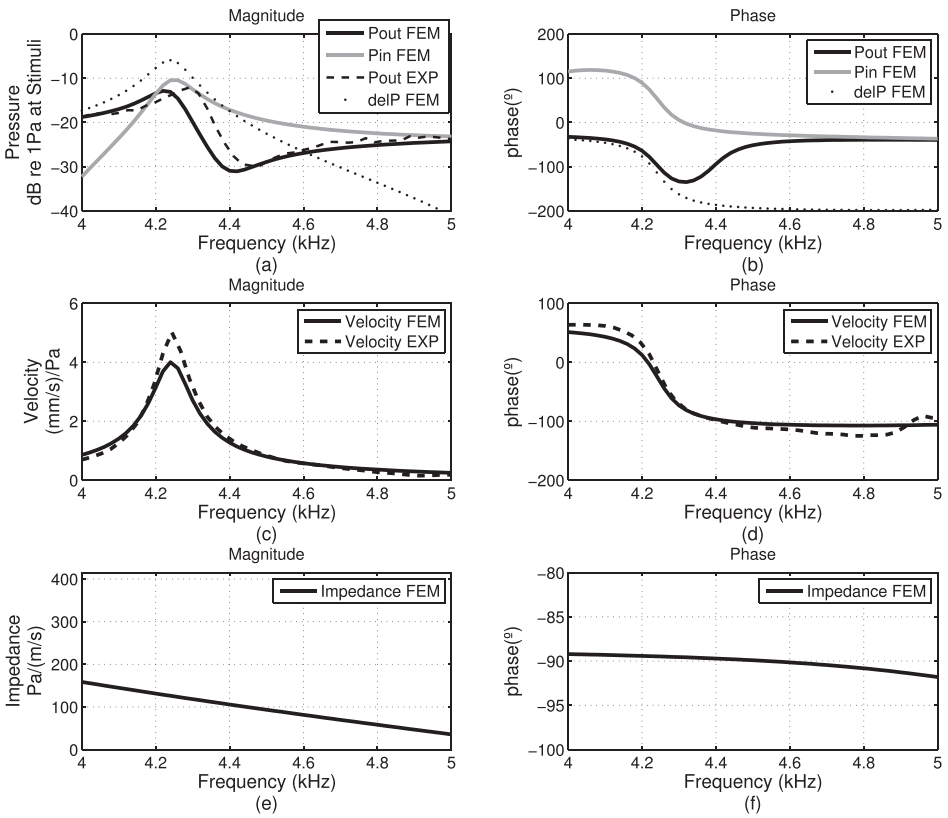

FIG. 10. FEM-calculated pressure and velocity at/of the center of the membrane in the membrane-tube system, plotted versus frequency. Dashed lines show experimental results when available. (a) and (b): Magnitude and phase of inside and outside pressures and pressure difference across the membrane. (c) and (d): Membrane velocity. (e) and (f): Membrane mechanical impedance.

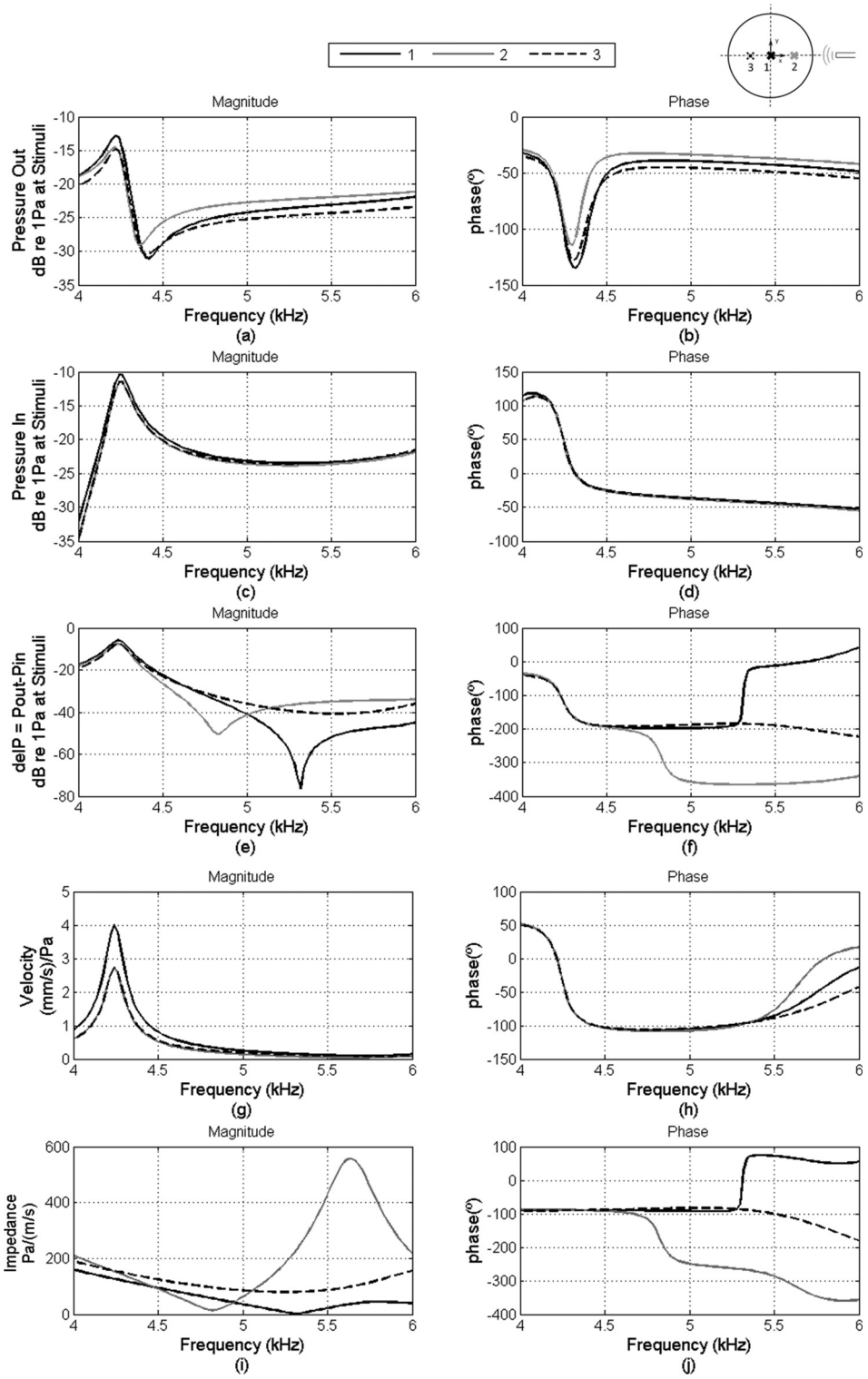

FIG. 11. Similar to Fig. 10 but three locations on the membrane are shown and the frequency range is extended. FEM results (magnitude and phase) of (a) and (b) pressure outside the membrane, (c) and (d) pressure inside the membrane, (e) and (f) pressure difference across the membrane, ΔP, (g) and (h) velocity of the membrane, (i) and (j) impedance of the membrane, found as ΔP/velocity.

applicable to this distributed system. Nevertheless, by examining the impedance at several locations and also the elements going into its calculation, the impedance values can be understood.

Continuing in this vein, in Fig. 12(a), $|Z|$ is shown at locations along the diameter of the membrane, for a frequency range 0–20 kHz. Figure 12(a) is for the tube-membrane system, and Fig. 12(b) for a baffle-membrane system. For any specific frequency, we can evaluate the distribution of Z along the diameter of the membrane. The diagram in the left upper corner indicates the axis of measurement with the colored crosses, and the positions along the diameter of the colored crosses are mapped to the colored horizontal lines in the main panels. Z_{air} [$\sim$415 Pa/(m/s)] serves as a useful reference value. There are frequencies for which $Z < Z_{air}$ for nearly the entire diameter, and frequencies for which Z is very low only in concentrated areas, but the average Z across the diameter is still $> Z_{air}$. Locating the frequencies where $Z < Z_{air}$ for the entire diameter, it is apparent that they occur at the mechanical resonance frequencies of

the membrane. The mechanical resonant frequencies are noted with the modal diagrams at the top and vertical gray lines. The radially symmetric modes (m1, m4, m9) are easily identified, while some of the modes (m3, m5, and m7) are relatively difficult to identify due to their axial nodes and the fact that only a single axis is illustrated in the figure.

We note that especially at the higher frequencies there is a slight discrepancy between the membrane resonant frequencies that emerge from Fig. 12, and the mode frequencies from the shell model in Table I. The resonant frequencies that are apparent in Fig. 12 are also tabulated in Table I in the row labeled, "solid element." The reason for the difference is numerical error. The natural frequencies shown in the shell model row of Table I were obtained with a FEM with shell elements with a reasonable mesh and small error. In contrast, the model used to solve the mechano-acoustic coupled problem was made with solid element as stated when describing the FEM and discussing Fig. 4. The element size selected was decided to simulate correct behavior for the range of frequency including the first few modes without excessive computational cost. That meant that at higher frequencies a small error was expected and accepted (following the trend shown in Fig. 6). This error produces a slightly increased stiffness and so predicts slightly higher resonant frequencies than the shell-element prediction. The differences in resonant frequencies found with solid elements, shells, or using the classical theory can be found in Table I. The small differences do not influence our findings significantly.

An important observation from Fig. 12(a) is that the influence of the tube resonance disappears. This is very clear at lower frequencies where the maximum observed at 1.5 kHz for velocity and pressure (Fig. 8) is not present. This is as expected because the mechanical impedance has been found using the pressures on the membrane and its motion——thus the membrane has been isolated, so the mechanical impedance is purely a property of the membrane. To emphasize this last point, the impedance has been computed for the case of the membrane with the baffle and

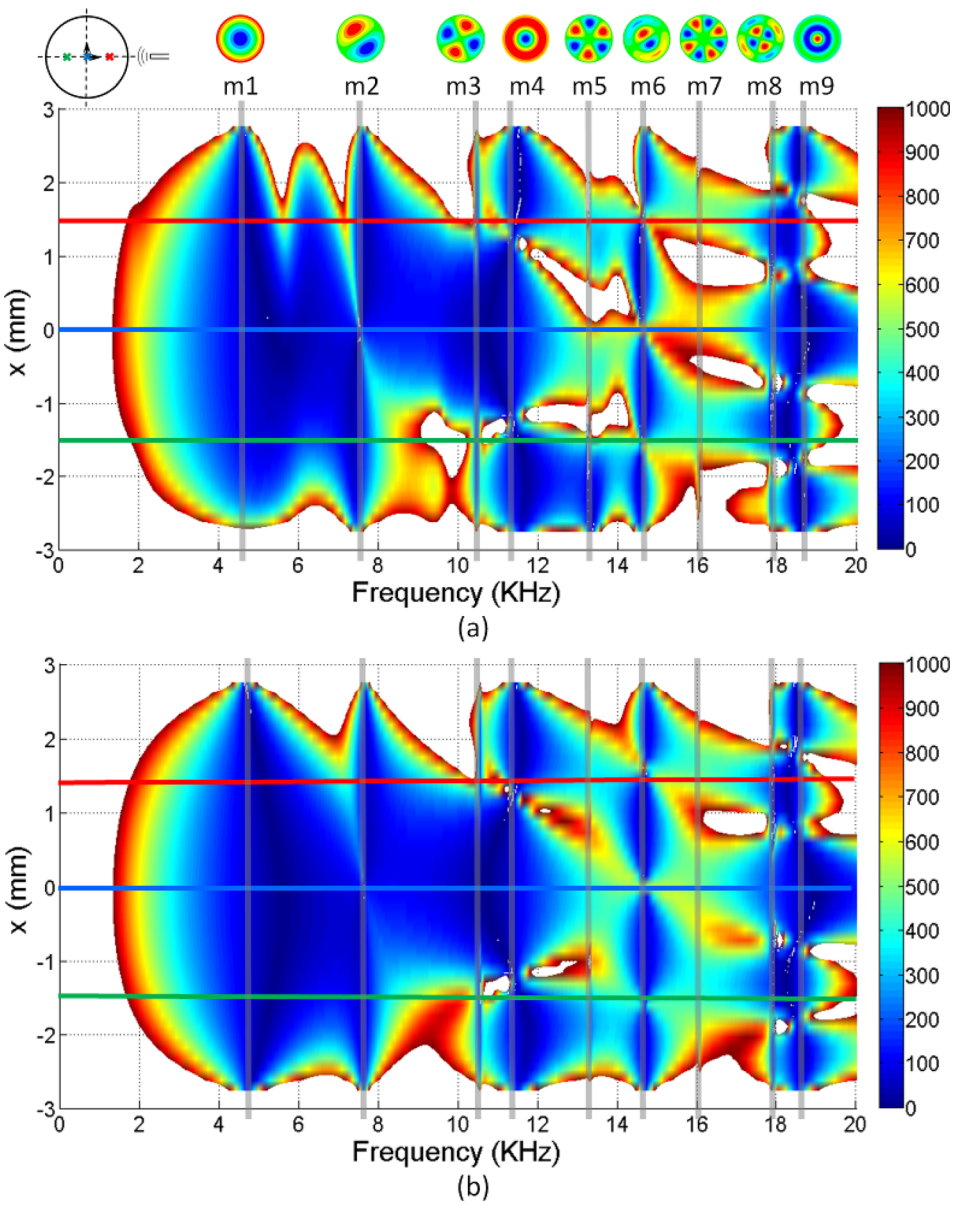

FIG. 12. (Color online) Impedance of the membrane, ΔP/velocity, versus frequency (horizontal axis) calculated along the diameter (vertical axis). The color code at the right gives the impedance in units of Pa/(m/s). White areas in the figure correspond to regions where the impedance was >1000 Pa/(m/s). The small circular diagram at the top left of the figure shows the diameter of the membrane along which the (calculated) data are plotted (that with the colored crosses), and the data at the positions of the crosses are noted by the horizontal colored lines in the figure. The small circular diagrams spanning the top of the figure show the membrane's mechanical modes. (The colors of the circular diagram are for illustration and not related to the color key at the right.) (a) Tube-membrane system (b) Baffle-membrane system.

without the tube, Fig. 12(b). The result is similar in the presence of either the tube or the baffle. While individual impedance values can be misleading, when the values spanning the diameter are considered, the figure clearly illustrates the mechanical resonances of the membrane alone.

IV. DISCUSSION

A. Significance of results for middle ear transmission

The systems under study have similar components to the middle ear system but were not arranged in the same way——in the middle ear, sound is delivered to the open end of a tube (EC) and the membrane (TM) is at the far end with the ME cavity behind. In our membrane-tube system, the sound was delivered to the membrane with the tube behind. The ME cavity was not included nor was the cochlear load. Nevertheless, the size and mechanics of the membrane were similar to that of the gerbil TM, which displays complex motion suggesting mechanical resonances starting in the kHz range (de La Rochefoucauld and Olson, 2010). The tube was of a length like that of the human EC. Thus basic aspects of the results are relevant to the ME system.

Several aspects of the results are of particular interest to ME mechanics. The pressure on the far side of the membrane commonly exceeded the pressure on the near, sound-source side. This occurred both due to quarter or three-quarter wave resonance [Figs. 9(b) and 9(e)] and due to mechanical resonance of the membrane [Figs. 9(d) and 9(f)]. The latter case corresponds to large membrane motion and considering this result with respect to the ME system, large TM motion would give rise to large MEC pressure. Intuitively, the presence of large MEC acoustic pressure might be considered to be detrimental to TM motion drive because we would expect a large external-internal pressure *difference* to be an effective drive. Indeed, there is typically a substantial pressure drop across the TM; in averaged measurements in gerbil, the internal pressure was typically at least 10 dB down compared to the external pressure (Fig. 3b of Bergevin and Olson, 2014). However, in the same study, in individual ears, there were frequency regions in which internal pressure exceeding external pressure by several decibels. Based on the results from current study, these regions are expected to correspond to relatively large TM motion.

In recent experimental work (Bergevin and Olson, 2014), reflections within the ME cavity were explored to probe theoretical predications from an abstract model in which cavity reflections were shown to extend the bandwidth of ME function (Rabbitt, 1990). Experimentally, standing wave patterns were observed within the ME cavity, signifying the presence of the predicted cavity reflections, but it was not clear if those reflections enhanced ME function. A FEM that includes the middle ear cavity in more anatomical detail would be of interest to explore this question further. The present study provides a good start for dealing with the numerical details of such a model, for example, the use of the hexahedral solid elements with enhanced strain formulation to provide efficient meshing at the membrane.

The results of the present study underscore the inescapability of acoustical and mechanical resonances in a system with properties like the ME. This is supportive of ME models that include resonances and predict that as long as there are many mistuned resonances, broad-band transmission of sound energy to the cochlea will occur (Funnell and Laszlo, 1978; Funnell *et al.*, 1987; Fay *et al.*, 2006). Damping in the membrane also helps produce broad-band transmission, by merging nearby resonances (Funnell *et al.*, 1987). Because ME transmission is high-fidelity and with short delay [$\sim$25 μs in gerbil (Olson, 1998)], there is not time for the resonances to build up, and it is probably not correct to think of these resonances as "useful" but rather as "unavoidable," and the presence of many mistuned resonances allows for the persistent ringing of the individual resonances to cancel out (Olson *et al.*, 2015).

Our abstract model is missing the most important component of the auditory system: the cochlea. The flow of acoustic power through the middle ear to the cochlea has been quantified through measurements of pressure and velocity (e.g., Rosowski *et al.*, 1986; Ravicz *et al.*, 1992, 1996), and an impressive fraction of the acoustic power available at the ear canal is absorbed by the cochlea. By absorbing sound energy, the cochlea damps the ME system. Although we are missing this fundamental component, our model's present components——acoustic spaces and a flexible, complexly moving membrane——are present in the ME, and the behavior of our simple model has counterparts in the experimental ME literature. In particular, the TM's complex, multi-phasic response to tonal stimuli, and its persistent ringing to click stimuli have been measured experimentally, and substantial pressure transmission through the TM at particular frequencies was recently documented. How the funneling of sound energy to the cochlea occurs, given the dynamic ME system it must navigate, remains to be understood, and is informed by our model results.

B. Conclusion

A simple mechano-acoustical system of a tube and membrane was studied via calculation on a numerical model. Only with a properly informed model, in which the system parameters are known, can we obtain accurate numerical data. This has been done in this work, which was supported by a complete set of experimental data, including both pressure and velocity. Using the numerical model, pressure and velocity were determined along a large spatial and frequency distribution. By considering the ratio of pressure difference across the membrane to velocity (the impedance), the mechanical resonances of the membrane alone were observed. As expected, the membrane-alone impedance was nearly independent of the acoustic environment——the pressure/velocity calculation yielded results that were much the same whether the tube + membrane or baffle + membrane system was considered. Frequencies where impedance was small over most of the diameter of the membrane coincided with the expected mechanical resonances of the membrane. At frequencies where the membrane impedance was low, the presence of the membrane increased the pressure amplitude on both sides of the membrane and decreased the pressure difference. Thus the system operated as a relatively open gate for sound

transmission at some frequencies, and a relatively closed gate at other frequencies. While our tube + membrane model was an extreme abstraction of the ME, the acousto-mechanical relationships we emphasize apply to the actual ME system and reinforce the significance of its dynamical properties.

ACKNOWLEDGMENTS

This work was supported by the Spanish Ministry of Education, Culture, and Sport, the University of Malaga, Spain, the NIDCD, and the Emil Capita Foundation. The paper benefited greatly from the comments of the JASA reviewers.

Andelfinger, U., and Ramm, E. (**1993**). "EAS-elements for two-dimensional, three-dimensional, plate and shell structures and their equivalence to HR-elements," Int. J. Num. Methods Eng. **36**, 1311–1337.

Bergevin, C., and Olson, E. S. (**2014**). "External and middle ear sound pressure distribution and acoustic coupling to the tympanic membrane," J. Acoust. Soc. Am. **135**, 1294–1312.

Cheng, J. T., Hamade, M., Merchant, S. N., Rosowski, J. J., Harrington, E., and Furlong, C. (**2013**). "Wave motion on the surface of the human tympanic membrane: Holographic measurement and modeling analysis," J. Acoust. Soc. Am. **133**, 918–937.

de La Rochefoucauld, O., and Olson, E. S. (**2010**). "A sum of simple and complex motions on the eardrum and manubrium in gerbil," Hear. Res. **263**, 9–15.

Fay, J. P., Puria, S., and Steele, C. R. (**2006**). "The discordant eardrum," PNAS **103**, 19743–19748.

Funnell, W. R. G., Decraemer, W. F., and Khanna, S. M. (**1987**). "On the damped frequency response of a FEM of the cat eardrum," J. Acoust. Soc. Am. **81**, 1851–1859.

Funnell, W. R. J., and Laszlo, C. A. (**1978**). "Modeling of the cat eardrum as a thin shell using the finite element method," J. Acoust. Soc. Am. **63**, 1461–1467.

Gonzalez-Herrera, A., Wattamwar, K., Bergevin, C., and Olson, E. S. (**2013**). "Sound transmission in a simple model of the ear canal and tympanic membrane," Acoust. Soc. Am. **19**, 030099.

Hall, D. E. (**1993**). *Basic Acoustics* (Krieger, Malagar, FL).

Keefe, D. H., Bulen, J. C., Arehart, K. C., and Burns, E. M. (**1993**). "Ear canal impedance and reflection coefficient in human infants and adults," J. Acoust. Soc. Am. **94**, 2617–2638.

Khanna, S., and Tonndorf, J. (**1972**). "Tympanic membrane vibrations in cats studied by time-averaged holography," J. Acoust. Soc. Am. **51**, 1904–1920.

Khanna, S. M., Koester, C. J., Willemin, J. F., Dandliker, R., and Rosskothen, H. (**1996**). "A noninvasive optical system for the study of the function of inner ear in living animals," SPIE **2732**, 64–81.

Kuypers, L. C., Dirckx, J. J. J., Decraemer, W. F., and Timmermans, J. P. (**2005**). "Thickness of the gerbil tympanic membrane measured with confocal microscopy," Hear. Res. **209**, 42–52.

Olson, E. S. (**1998**). "Observing middle and inner ear mechanics with novel intracochlear pressure sensors," J. Acoust. Soc. Am. **103**, 3445–3463.

Olson, E. S., Kumar, N., Lei, J., and Bergevin, C. (**2015**). "The role of resonance in middle ear transmission," *Abstracts of the 38th Midwinter Research Meeting*, Association for Research in Otolaryngology.

Puria, S., and Allen, J. B. (**1998**). "Measurements and model of the cat middle ear, evidence of tympanic membrane delay," J. Acoust. Soc. Am. **104**, 3463–3481.

Rabbitt, R. D. (**1990**). "A hierarchy of examples illustrating the acoustic coupling of the eardrum," J. Acoust. Soc. Am. **87**, 2566–2582.

Ravicz, M., Rosowski, J., and Voigt, H. (**1992**). "Sound-power collection by the auditory periphery of the Mongolian gerbil *Meriones unguiculatus*. I. Middle ear input impedance," J. Acoust. Soc. Am. **92**, 157–177.

Ravicz, M., Rosowski, J., and Voigt, H. (**1996**). "Sound-power collection by the auditory periphery of the Mongolian gerbil *Meriones unguiculatus*. II. External-ear radiation impedance and power collection," J. Acoust. Soc. Am. **99**, 3044–3063.

Ravicz, M. E., Olson, E. S., and Rosowski, J. J. (**2007**). "Sound pressure distribution and power flow within the gerbil ear canal form 100 to 80 kHz," J. Acoust. Soc. Am. **122**, 2154–2173.

Rosowski, J. J., Carney, L. H., Lynch, T. J. III, and Peake, W. T. (**1986**). "The effectiveness of external and middle ears in coupling acoustic power into the cochlea," in *Peripheral Auditory Mechanisms*, edited by J. B. Allen, J. L. Hall, A. Hubbard, S. T. Neely, and A. Tubis (Springer, New York), pp. 3–12.

Sakurada, I., Kaji, K., and Wadano, S. (**1981**). "Elastic moduli and structure of low density polyethylene," Colloid Polymer Sci. **259**, 1208–1213.

Simo, J. C., Armero, F., and Taylor, R. L. (**1993**). "Improved versions of assumed enhanced strain tri-linear elements for 3D finite deformation problems," Comput. Methods Appl. Mech. Eng. **110**, 359–386.

Simo, J. C., and Rifai, M. S. (**1990**). "A class of mixed assumed strain methods and the method of incompatible modes," Int. J. Num. Methods Eng. **29**, 1595–1638.

Stinson, M. R. (**1985**). "The spatial distribution of sound pressure within scaled replicas of the human ear canal," J. Acoust. Soc. Am. **78**, 1596–1602.